# Fast Euler Solver for Transonic Airfoils Part I: Theory

Andrea Dadone*
*University of Bari, Bari, Italy*
and
Gino Moretti†
*GMAF, Inc., Freeport, New York*

**An implicit Euler solver, based on the λ-formulation, is presented. Integration of the equations, written in terms of generalized Riemann variables, is performed by inverting six bidiagonal matrices and two tridiagonal matrices. Shocks are fitted. The solution is found on a *C* grid, the boundaries of which are very close to the airfoil.**

## I. Introduction

FOR a fast and accurate calculation of steady, supercritical flows about airfoils, the following conditions must be met:

1) Simple algorithms for the integration of the discretized Euler equations.
2) Reduction of the computational domain to a minimum.
3) Most efficient handling of boundary conditions.
4) High rate of convergence.
5) Accurate evaluation of the shocks.
6) Vectorizability.
7) Absence of "fine tuning" parameters.

The finite-volume, Runge–Kutta integrating scheme of Schmidt and Jameson[1] certainly satisfies conditions 1) and 6). In principle, since the code deals with the Euler equations in divergence form, the shocks should be properly located. This is not necessarily true, however; artificial viscosity terms that must be added to provide monotonicity smear out the shock transition over not less than three mesh intervals, and the location of the shock ends up being defined with a certain degree of arbitrariness. Consequently, the resulting drag coefficient loses accuracy. A refinement of the mesh is necessary for a better resolution of the shock; inevitably, the computational time increases. To satisfy condition 4), multigrid devices are used, which introduce yet another set of fine-tuning parameters.

We claim that the method described in this paper satisfies all of the foregoing seven conditions. The method relies on the λ-formulation of the Euler equations and the explicit fitting of shocks.[2] Computational speed is obtained by updating four generalized Riemann variables using four simple equations, in the spirit of Refs. 3–5. As formulated in Ref. 5, however, the method is redundant. To provide consistency, certain terms are redefined and convergence is assured. The accuracy, proper of the λ-schemes, is enhanced by the use of the COIN technique[6] and shock fitting. Neither device adds a substantial time to what would be required by a straightforward calculation of a shockless flow.

## II. General Equations

We consider a polytropic, inviscid gas with a constant ratio of specific heats $\gamma$. For simplicity of notation, we define

$$\delta = (\gamma - 1)/2 \tag{1}$$

In what follows, $a$ denotes the speed of sound, $S$ the entropy, and $q$ the velocity vector. All velocities are nondimensionalized if we assume the square root of the ratio between pressure and density at infinity is the unity of speed. In nondimensional form, the pressure $p$, density $\rho$, and temperature $T$ are related by

$$p = \rho T \tag{2}$$

and entropy is defined as

$$S = (\tfrac{1}{2}\gamma\delta)\, \ell n\, (p/\rho^{\gamma}) \tag{3}$$

As in Ref. 2, the nondimensional equations expressing conservation of entropy, mass, and momentum are given, in vector form, as

$$S_t + \boldsymbol{q} \cdot \nabla S = 0$$

$$a_t/\delta + \boldsymbol{q} \cdot \nabla a/\delta + a\nabla \cdot \boldsymbol{q} - aS_t - a\boldsymbol{q} \cdot \nabla S = 0$$

$$\boldsymbol{q}_t + (\boldsymbol{q} \cdot \nabla)\boldsymbol{q} + a\nabla a/\delta - a^2 \nabla S = 0 \tag{4}$$

## III. Equations in Gradient Form

We recall some of the notations used in Ref. 2. At any node of a computational grid in the physical plane, we choose two unit vectors, $\boldsymbol{n}$ and $\tau$, perpendicular to one another. Let $\alpha_0$ be the angle between $\boldsymbol{n}$ and a fixed direction in the physical plane. Let

$$\boldsymbol{q} = u\boldsymbol{n} + v\tau \tag{5}$$

and

$$\rho_1 = a/\delta + u, \qquad \Lambda_1 = \boldsymbol{q} + a\boldsymbol{n}$$

$$\rho_2 = a/\delta - u, \qquad \Lambda_2 = \boldsymbol{q} - a\boldsymbol{n}$$

$$\rho_3 = a/\delta + v, \qquad \Lambda_3 = \boldsymbol{q} + a\tau$$

$$\rho_4 = a/\delta - v, \qquad \Lambda_4 = \boldsymbol{q} - a\tau \tag{6}$$

and

$$\beta = \boldsymbol{q} \cdot \nabla\alpha_0, \qquad F = a\boldsymbol{k} \cdot \boldsymbol{q} \cdot \nabla\alpha_0 \tag{7}$$

where $\boldsymbol{k}$ is a unit vector, orthogonal to the physical plane, and

$$D = a\tau \cdot \nabla v, \qquad E = a\boldsymbol{n} \cdot \nabla u \tag{8}$$

Received April 13, 1987; revision received Aug. 20, 1987.

*Professor, Istituto di Macchine ed Energetica.
†Consultant. Fellow AIAA.

By combining the second and third equations of Ref. 4, the following equations are obtained, which can be interpreted as compatibility conditions along four bicharacteristics:[2]

$$\rho_{1t} - aS_t + \Lambda_1 \cdot (\nabla\rho_1 - a\nabla S) + D - \beta v + F = 0 \quad (9a)$$

$$\rho_{2t} - aS_t + \Lambda_2 \cdot (\nabla\rho_2 - a\nabla S) + D + \beta v + F = 0 \quad (9b)$$

$$\rho_{3t} - aS_t + \Lambda_3 \cdot (\nabla\rho_3 - a\nabla S) + E + \beta u + F = 0 \quad (9c)$$

$$\rho_{4t} - aS_t + \Lambda_4 \cdot (\nabla\rho_4 - a\nabla S) + E - \beta u + F = 0 \quad (9d)$$

In Ref. 2, these four equations are combined to produce three equations for $a_t$, $u_t$, and $v_t$ as follows:

$$4a_t/\delta - 4aS_t + 4a\boldsymbol{q} \cdot \nabla S + 2\Sigma\Lambda_i \cdot (\nabla\rho_i - a\nabla S) - 4\boldsymbol{q} \cdot \nabla a/\delta + 4F = 0 \quad (10)$$

$$2u_t + \Lambda_1 \cdot (\nabla\rho_1 - a\nabla S) - \Lambda_2 \cdot (\nabla\rho_2 - a\nabla S) - 2\beta v = 0 \quad (11)$$

$$2v_t + \Lambda_3 \cdot (\nabla\rho_3 - a\nabla S) - \Lambda_4 \cdot (\nabla\rho_4 - a\nabla S) + 2\beta u = 0 \quad (12)$$

plus the obvious identity

$$\rho_{1t} + \rho_{2t} - \rho_{3t} - \rho_{4t} = 0 \quad (13)$$

Here instead, in the spirit of Ref. 5, we want to maintain Eqs. (9a–9d) as they are, because the symmetry of Eqs. (9) and the simplicity of each equation speeds up the numerical procedure. The identity of Eqs. (9a–9d) and (10–13) is not necessarily preserved in a numerical computation. The first two equations, indeed, define $u_t$ and $a_t$, and the last two equations define $v_t$ and $a_t$ again, so that $a_t$ is defined twice, independently, and the numerical results are not necessarily identical. Numerical experiments proved, indeed, that the values of $a$, computed from the first two equations or the last two equations, may differ by a small amount (of the order of 0.001), which is mesh-dependent.

This redundancy occurs because, in Ref. 5, $D$ and $E$ are numerically evaluated using the gradients of $u$ and $v$. Conversely, here we want to express $D$ and $E$ directly in terms of *gradients* of the Riemann variables and $S$, in such a way that, when their expressions are replaced into Eq. (9), the new system becomes identical with Eqs. (10–13), analytically as well as numerically. Such a condition is already identically satisfied for Eqs. (11) and (12); we can prove it simply by subtracting Eq. (9b) from Eq. (9a), the first, and by subtracting Eq. (9d) from Eq. (9c). As for Eqs. (10) and (13), we begin by noting that the sum of the four equations in Eq. (9) defines $a_t$; $a_t$ is also defined by Eq. (10). To establish the identity of the two expressions, the following condition must be satisfied:

$$-\sum_1^4 \Lambda_i \cdot (\nabla\rho_i - a\nabla S) + 2(D+E) + 4\boldsymbol{q} \cdot (\nabla a/\delta - a\nabla S) = 0 \quad (14)$$

On the other hand, if we subtract the sum of the last two equations in Eq. (9) from the sum of the first two, we see that Eq. (13) is satisfied if

$$\sum_1^2 [\Lambda_i \cdot (\nabla\rho_i - a\nabla S) - \Lambda_{i+2} \cdot (\nabla\rho_{i+2} - a\nabla S)] + 2(D-E) = 0 \quad (15)$$

From Eqs. (14) and (15), $D$ and $E$ are obtained

$$2D = \sum_3^4 \Lambda_i \cdot (\nabla\rho_i - a\nabla S) - 2\boldsymbol{q} \cdot (\nabla a/\delta - a\nabla S)$$

$$2E = \sum_1^2 \Lambda_i \cdot (\nabla\rho_i - a\nabla S) - 2\boldsymbol{q} \cdot (\nabla a/\delta - a\nabla S) \quad (16)$$

At this stage, we can discretize our current equations and show that, by proper algebraic manipulations, they become identical with the discretized forms of Eqs. (10–12).

## IV. Orthogonal Frames

Let $\xi$ and $\eta$ be two orthogonal coordinates, $h_1$ and $h_2$ their metric parameters, and $g_1 = 1/h_1$, $g_2 = 1/h_2$. With $\boldsymbol{n}$ and $\boldsymbol{\tau}$ along coordinate lines in the physical plane, the gradient of any function $W$ is

$$\nabla W = g_1 W_\xi \boldsymbol{n} + g_2 W_\eta \boldsymbol{\tau} \quad (17)$$

so that the gradient of $\alpha_0$ can be expressed as

$$\nabla\alpha_0 = g_1 g_2 (h_{2\xi}\boldsymbol{\tau} - h_{1\eta}\boldsymbol{n}) \quad (18)$$

Therefore,

$$\Phi = g_1 g_2 (h_{2\xi} u + h_{1\eta} v), \qquad F = a\Phi \quad (19)$$

$$\beta = g_1 g_2 (h_{2\xi} v - h_{1\eta} u) \quad (20)$$

We define

$$R_1^X = \rho_1 = a/\delta + u; \quad R_2^X = \rho_2 = a/\delta - u$$

$$R_1^Y = \rho_3 = a/\delta + v, \quad R_2^Y = \rho_4 = a/\delta - v \quad (21)$$

$$\lambda_1^X = g_1(u+a), \quad \lambda_2^X = g_1(u-a), \quad \lambda_3^X = g_1 u$$

$$\lambda_1^Y = g_2(v+a), \quad \lambda_2^Y = g_2(v-a), \quad \lambda_3^Y = g_2 v \quad (22)$$

(in nonorthogonal coordinates, the $\rho$ and $R$ of Eq. (21) are not identical; see Ref. 2). Therefore,

$$\Lambda_1 = \lambda_1^X \boldsymbol{n} + \lambda_3^Y \boldsymbol{\tau}, \qquad \Lambda_2 = \lambda_2^X \boldsymbol{n} + \lambda_3^Y \boldsymbol{\tau},$$

$$\Lambda_3 = \lambda_3^X \boldsymbol{n} + \lambda_1^Y \boldsymbol{\tau}, \qquad \Lambda_4 = \lambda_3^X \boldsymbol{n} + \lambda_2^Y \boldsymbol{\tau}, \quad (23)$$

Note that

$$\sum_1^4 \Lambda_i \cdot \nabla\rho_i - (2/\delta)\boldsymbol{q} \cdot \nabla a = \sum_1^2 (\lambda_i^X R_{i\xi}^X + \lambda_i^Y R_{i\eta}^Y) \quad (24)$$

$$-\sum_1^4 \Lambda_i \cdot a\nabla S + 2a\boldsymbol{q} \cdot \nabla S = -\sum_1^2 (\lambda_i^X a S_\xi + \lambda_i^Y a S_\eta) \quad (25)$$

From Eqs. (24) and (25), it follows that

$$\sum_1^4 \Lambda_i \cdot (\nabla\rho_i - a\nabla S) - 2\boldsymbol{q} \cdot (\nabla a/\delta - a\nabla S) = \sum_1^2 [\lambda_i^X (R_{i\xi}^X - aS_\xi) + \lambda_i^Y (R_{i\eta}^Y - aS_\eta)] \quad (26)$$

By comparison with the first part of Eq. (16), we obtain

$$\sum_1^2 \Lambda_i \cdot (\nabla R_i^X - a\nabla S) + 2D = \sum_1^2 [\lambda_i^X (R_{i\xi}^X - aS_\xi) + \lambda_i^Y (R_{i\eta}^Y - aS_\eta)] \quad (27)$$

On the other hand,

$$\sum_1^2 \Lambda_i \cdot (\nabla R_i^X - a\nabla S) = \sum_1^2 [\lambda_i^X (R_{i\xi}^X - aS_\xi) + \lambda_3^Y (R_{i\eta}^X - aS_\eta)] \quad (28)$$

From Eqs. (27) and (28), the equation for $D$ follows in its final form

$$D = \frac{1}{2}\{\lambda_1^Y (R_{1\eta}^Y - aS_\eta) + \lambda_2^Y (R_{2\eta}^Y - aS_\eta) - \lambda_3^Y [(R_{1\eta}^X - aS_\eta) + (R_{2\eta}^X - aS_\eta)]\} \quad (29)$$

Similarly,

$$E=\frac{1}{2}\{\lambda_1^X(R_{1\xi}^X-aS_\xi)+\lambda_2^X(R_{2\xi}^X-aS_\xi)$$
$$-\lambda_3^X[(R_{1\xi}^Y-aS_\xi)+(R_{2\xi}^Y-aS_\xi)]\} \tag{30}$$

To summarize, the equations to be integrated are

$$S_t+\lambda_3^X S_\xi+\lambda_3^Y S_\eta=0 \tag{31}$$

$$R_{1t}^X-aS_t+\lambda_1^X(R_{1\xi}^X-aS_\xi)+\lambda_3^Y(R_{1\eta}^X-aS_\eta)$$
$$+D-\beta v+a\Phi=0 \tag{32a}$$

$$R_{2t}^X-aS_t+\lambda_2^X(R_{2\xi}^X-aS_\xi)+\lambda_3^Y(R_{2\eta}^X-aS_\eta)$$
$$+D+\beta v+a\Phi=0 \tag{32b}$$

$$R_{1t}^Y-aS_t+\lambda_1^Y(R_{1\eta}^Y-aS_\eta)+\lambda_3^X(R_{1\xi}^Y-aS_\xi)$$
$$+E-\beta u+a\Phi=0 \tag{32c}$$

$$R_{2t}^Y-aS_t+\lambda_2^Y(R_{2\eta}^Y-aS_\eta)+\lambda_3^X(R_{2\xi}^Y-aS_\xi)$$
$$+E-\beta u+a\Phi=0 \tag{32d}$$

with $D$, $E$, $\beta$, and $\Phi$ defined by Eqs. (29), (30), (20), and (19), respectively.

## V. COIN Variant

To minimize errors in the leading-edge region and a consequent decay of total temperature on the surface of the airfoil, we reformulate Eqs. (31) and (32) in the spirit of Ref. 6. Let us split $q$ and $a$ into sums of two terms, of which those denoted by the superscript $^0$ are computed at the start of the calculation and never changed again, and those denoted by a prime are the unknowns be to computed

$$q=q^0+q', \qquad a=a^0+a' \tag{33}$$

The velocity $q^0$ is the velocity of an incompressible, irrotational flow about the profile; therefore, it satisfies the conditions

$$\nabla\cdot q^0=0, \qquad \nabla\times q^0=0 \tag{34}$$

The term $a^0$ is related to $q^0$ by the condition of conservation of total temperature

$$\delta(q^0)^2+(a^0)^2=a_0^2=a_\infty^2(1+\delta M_\infty^2) \tag{35}$$

where $a_0$ is the stagnation speed of sound, and $a_\infty$, $M_\infty$ are the values of $a$ and $M$ at infinity. As said previously, neither $q^0$ nor $a^0$ depends on time

$$q_t^0=0, \qquad a_t^0=0 \tag{36}$$

For brevity, we denote the following technique by the acronym COIN (compressible over incompressible). In the vicinity of the leading edge, where the flow stagnates, a compressible flow behaves as incompressible; therefore, better accuracy will be obtained in discretizing the primed terms since their gradients are small.[6]

All "incompressible" velocities are obtained by solving Eq. (34) and prescribing a velocity at infinity $V_\infty^0$. The actual velocity at infinity is $V_\infty=a_\infty M_\infty$ but, instead of letting $V_\infty^0=V_\infty$ (which with the current nondimensionalizing parameters would make $V_\infty^0=\sqrt{\gamma}M_\infty$), we first compute the ratio, density/stagnation density at infinity [which, in this context, is $1/(1+\delta M_\infty^2)^{1/(\gamma-1)}$] and then define

$$V_\infty^0=\sqrt{\gamma}M_\infty/(1+\delta M_\infty^2)^{1/(\gamma-1)} \tag{37}$$

By so doing, mass flows in the stagnation region are well represented by the incompressible solution.

We also split $\beta$ into a sum $\beta^0+\beta'$, and $\Phi$ into a sum $\Phi^0+\Phi'$. Similar splits are made for the quantities defined by Eqs. (21) and (22). Conditions (34) can now be written in the form

$$\Phi^0+g_1u_\xi^0+g_2v_\eta^0=0 \tag{38}$$

$$\beta^0+g_1v_\xi^0-g_2u_\eta^0=0 \tag{39}$$

After performing similar splittings of terms in Eqs. (29) and (30), we can regroup the terms and use Eqs. (38) and (39) to simplify the expressions. The results can be written in the form

$$D=g_2a^0v_\eta^0+g_2a'v_\eta^0+D^* \tag{40}$$

$$E=g_1a^0\mu_\xi^0+g_1a'u_\xi^0+E^* \tag{41}$$

with

$$D^*=\frac{1}{2}\{\lambda_1^Y(R_{1\eta}'^Y-aS_\eta)+\lambda_2^Y(R_{2\eta}'^Y-aS_\eta)$$
$$-\lambda_3^Y[(R_{1\eta}'^X-aS_\eta)+(R_{2\eta}'^X-aS_\eta)]\}$$
$$E^*=\frac{1}{2}\{\lambda_1^X(R_{1\xi}'^X-aS_\xi)+\lambda_2^X(R_{2\xi}'^X-aS_\xi)$$
$$-\lambda_3^X[(R_{1\xi}'^Y-aS_\xi)+(R_{2\xi}'^Y-aS_\xi)]\} \tag{42}$$

(Note the mixture of primed, differentiated terms and nonprimed coefficients in $D^*$ and $E^*$.) Eq. (32a) is now written

$$R_{1t}'^X-aS_t+\lambda_1^{0X}R_{1\xi}^{0X}+\lambda_1'^XR_{1\xi}^{0X}+\lambda_1^X(R_{1\xi}'^X-aS_\xi)$$
$$+\lambda_3^{0Y}R_{1\eta}^{0X}+\lambda_3'^YR_{1\eta}^{0X}+\lambda_3^Y(R_{1\eta}'^X-aS_\eta)+D^*$$
$$+g_2a^0v_\eta^0+g_2a'v_\eta^0-\beta^0v^0-\beta^0v'-\beta'v^0-\beta'v'$$
$$+a^0\Phi^0+a^0\Phi'+a'\Phi^0+a'\Phi'=0 \tag{43}$$

The identity

$$\lambda_1^{0X}R_{1\xi}^{0X}+\lambda_3^{0Y}R_{1\eta}^{0X}+g_2a^0v_\eta^0-\beta^0v^0+a^0\Phi^0$$
$$=(g_1u^0a_\xi^0+g_2v^0a_\eta^0)/\delta \tag{44}$$

is easily verified, using Eqs. (35), (38), and (39), and it is used to simplify Eq. (43). Other terms in Eq. (43), having $a'$ or $v'$ as a common factor and no other primed factors, are eliminated using Eqs. (38) or (39), respectively. Thus, we may write, in lieu of Eq. (43)

$$R_{1t}'^X-aS_t+\lambda_1^X(R_{1\xi}'^X-aS_\xi)+\lambda_3^Y(R_{1\eta}'^X-aS_\eta)$$
$$+a'\Phi'-\beta'v'+D^*$$
$$+g_1u'[g_2(h_{2\xi}a^0+h_{1\eta}v^0)+a_\xi^0/\delta+u_\xi^0]$$
$$+g_2v'[g_1(h_{1\eta}a^0-h_{2\xi}v^0)+a_\eta^0/\delta+g_1h_2v_\xi^0]$$
$$+g_1a'a_\xi^0/\delta+(g_1u^0a_\xi^0+g_2v^0a_\eta^0)/\delta=0 \tag{45}$$

Similar expressions are found for Eqs. (32b–32d). To retain some analogy with the symbols used in Ref. 2, we define

$$f_1^X = -\lambda_1^X(R_{1\xi}'^X - aS_\xi), \quad f_1^Y = -\lambda_1^Y(R_{1\eta}'^Y - aS_\eta)$$

$$f_2^X = -\lambda_2^X(R_{2\xi}'^X - aS_\xi), \quad f_2^Y = -\lambda_2^Y(R_{2\eta}'^Y - aS_\eta)$$

$$f_{31}^X = -\lambda_3^X(R_{1\xi}'^Y - aS_\xi), \quad f_{31}^Y = -\lambda_3^Y(R_{1\eta}'^X - aS_\eta)$$

$$f_{32}^X = -\lambda_3^X(R_{2\xi}'^Y - aS_\xi), \quad f_{32}^Y = -\lambda_3^Y(R_{2\eta}'^X - aS_\eta)$$

$$f_4^X = -\lambda_3^X S_\xi, \quad f_4^Y = -\lambda_3^Y S_\eta \tag{46}$$

plus terms carrying local contributions

$$f_1^L = -a'\Phi' + \beta' v', \quad f_2^L = -a'\Phi' - \beta' v'$$

$$f_3^L = -a'\Phi' - \beta' u', \quad f_4^L = -a'\Phi' + \beta' u' \tag{47}$$

and corrective terms, expressed as linear combinations of $a'$, $u'$, and $v'$, with coefficients depending on incompressible terms (which can be evaluated once and for all at the beginning of the computation)

$$f_1^P = -A_{11}u' - A_{12}v' - A_{13}a' - A_4$$

$$f_2^P = -A_{21}u' - A_{22}v' - A_{23}a' - A_4$$

$$f_3^P = -A_{31}u' - A_{32}v' - A_{33}a' - A_4$$

$$f_4^P = -A_{41}u' - A_{42}v' - A_{43}a' - A_4 \tag{48}$$

with

$$A_{11} = g_1[g_2(h_{2\xi}a^0 + h_{1\eta}v^0) + a_\xi^0/\delta + u_\xi^0]$$

$$A_{12} = g_2[g_1(h_{1\eta}a^0 - h_{2\xi}v^0) + a_\eta^0/\delta] + g_1 v_\xi^0$$

$$A_{13} = g_1 a_\xi^0/\delta$$

$$A_{21} = g_1[g_2(h_{2\xi}a^0 - h_{1\eta}v^0) + a_\xi^0/\delta - u_\xi^0]$$

$$A_{22} = g_2[g_1(h_{1\eta}a^0 + h_{2\xi}v^0) + a_\eta^0/\delta] - g_1 v_\xi^0$$

$$A_{23} = -A_{13}$$

$$A_{31} = g_1[g_2(h_{2\xi}a^0 - h_{1\eta}u^0) + a_\xi^0/\delta] + g_2 u_\eta^0$$

$$A_{32} = g_2[g_1(h_{1\eta}a^0 + h_{2\xi}u^0) + a_\eta^0/\delta + v_\eta^0]$$

$$A_{33} = g_2 a_\eta^0/\delta$$

$$A_{41} = g_1[g_2(h_{2\xi}a^0 + h_{1\eta}u^0) + a_\xi^0/\delta] - g_2 u_\eta^0$$

$$A_{42} = g_2[g_1(h_{1\eta}a^0 - h_{2\xi}u^0) + a_\eta^0/\delta - v_\eta^0]$$

$$A_{43} = -A_{33}, \quad A_4 = (g_1 u^0 a_\xi^0 + g_2 v^0 a_\eta^0)/\delta \tag{49}$$

The final equations to be integrated in the COIN version [in lieu of Eqs. (31) and (32)] are

$$S_t = f_4^X + f_4^Y \tag{50}$$

$$R_{1t}'^X = aS_t + f_1^X + f_{31}^Y + f_1^L + f_1^P - D^*$$

$$R_{2t}'^X = aS_t + f_2^X + f_{32}^Y + f_2^L + f_2^P - D^*$$

$$R_{1t}'^Y = aS_t + f_1^Y + f_{31}^X + f_3^L + f_3^P - E^*$$

$$R_{2t}'^Y = aS_t + f_2^Y + f_{32}^X + f_4^L + f_4^P - E^* \tag{51}$$

where

$$D^* = -\frac{1}{2}(f_1^Y + f_2^Y + f_{31}^Y - f_{32}^Y)$$

$$E^* = -\frac{1}{2}(f_1^X + f_2^X + f_{31}^X - f_{32}^X) \tag{52}$$

Numerical experiments, to be reported by Dadone elsewhere, have shown that the COIN technique is efficient also when the compressible stagnation point is in the vicinity of, but not coincident with, the incompressible one (because the important gradients are in the direction normal to the body, not along the body itself).

## VI. Grid Generation

The grid used for all the present calculations is basically the same $C$ grid used in Ref. 5, with additional provisions for the mapping of arbitrarily shaped airfoils. The same grid has also been used in Ref. 7. From a Cartesian grid in a $\zeta$ plane ($\zeta = \xi + i\eta$), a $C$ grid is obtained in the physical $z$ plane ($z = x + iy$) through a set of transformations

$$Z = e\zeta, \qquad z_4^2 = b(Z-1)/(Z+1)$$

$$z_3 = \sqrt{(z_4-1)/(z_4+1)}, \qquad z_2 = (1+z_3)/(1-z_3)$$

$$z = z(z_2) \tag{53}$$

where $z(z_2)$ is, for a Joukowski profile, given by

$$z_1 = AC(z_2^2 - 1) + B, \qquad z = z_1 + 1/z_1 \tag{54}$$

with $A$ a thickness factor, $C$ a (complex) camber factor, and $B = 1 - AC$. In general, $z(z_2)$ is a combination of a von Kármán-Trefftz transformation and the Theodorsen mapping of a quasicircle on a circle. If we call $x_A$ and $x_C$ the abscissas of the left and right intersections of the grid outer boundary with the $x$ axis and use Eq. (53), two values $\eta_1(x_A)$ and $\xi_1(x_C)$ can be found. The computational rectangle in the $\zeta$ plane covers the area between $-\xi_1 < \xi < \xi_1$ and $0 < \eta < \eta_1$. With

$$g = Ge^{i\omega} = \frac{d\zeta}{dz} \tag{55}$$

$$\phi = \phi_1 + i\,\phi_2 = \frac{d \log g}{d\zeta} \tag{56}$$

it follows that

$$g_1 = g_2 = G \tag{57}$$

$$h_{1\xi} = h_{2\xi} = -\phi_1/G, \qquad h_{1\eta} = h_{2\eta} = \phi_2/G \tag{58}$$

$$\nabla\alpha_0 = -G(\phi_2 n + \phi_1 \tau) \tag{59}$$

$$\Phi = G(v\phi_2 - u\phi_1) \tag{60}$$

$$\beta = -G(v\phi_1 + u\phi_2) \tag{61}$$

Replacement of Eqs. (57) and (58) in Eq. (49) allows the coefficients $A_{ij}$ ($i, j = 1, 2, 3$) and $A_4$ to be simplified.

In addition, two independent stretchings of coordinates can be used to provide a better distribution of grid lines, with a concentration of lines in the vicinity of the airfoil and in the vicinity of the leading and, if necessary, of the trailing edge.

## VII. Implicit Formulation

Let us consider an integration step from a time $k\Delta t$ to a time $(k+1)\Delta t$. In the spirit of Ref. 2, we stipulate that all of

the derivatives in the $f_i^X$ terms at a point $P(n\Delta\xi, m\Delta\eta)$ are to be approximated by one-sided differences, taken between $P$ and the point $[(n-1)\Delta\xi, m\Delta\eta]$ if $\lambda_i^X > 0$, and between $P$ and the point $[(n+1)\Delta\xi, m\Delta\eta]$ if $\lambda_i^X < 0$. Similarly, all derivatives in the $f_i^Y$ terms are to be approximated by one-sided differences, taken between $P$ and the point $[n\Delta\xi, (m-1)\Delta\eta]$ if $\lambda_i^Y > 0$, and between $P$ and the point $[n\Delta\xi, (m+1)\Delta\eta]$ if $\lambda_i^Y < 0$. In addition, we recast Eqs. (50) and (51), introducing Beam and Warming's $\Delta$ form[8] for the most relevant terms in the right-hand sides. Here, $\Delta R'$ means the difference between the values of $R'$ at two successive time steps, at the same grid node. The procedure, already applied in Ref. 9, is shown in detail in the first part of Eq. (51). Since, for $\lambda_1^X > 0$,

$$(f_1^X)^{k+1} = -(\lambda_1^X)^k[R'^X_{1(n)} - R'^X_{1(n-1)}]^{k+1}/\Delta\xi + (\lambda_1^X)^k a^k S_\xi^k$$
$$= -(\lambda_1^X)^k[\Delta R'^X_{1(n)} - \Delta R'^X_{1(n-1)}]/\Delta\xi + (f_1^X)^k \quad (62)$$

and, for $\lambda_1^X < 0$,

$$(f_1^X)^{k+1} = -(\lambda_1^X)^k[R'^X_{1(n+1)} - R'^X_{1(n)}]^{k+1}/\Delta\xi + (\lambda_1^X)^k a^k S_\xi^k$$
$$= -(\lambda_1^X)^k[\Delta R'^X_{1(n)} - \Delta R'^X_{1(n+1)}]/\Delta\xi + (f_1^X)^k \quad (63)$$

the first part of Eq. (51) can be written in the form

$$A_n \Delta R'^X_{1(n-1)} + B_n \Delta R'^X_{1(n)} + C_n \Delta R'^X_{1(n+1)} = D_n \quad (64)$$

where

$$A_n = -\frac{1}{2}\frac{(\lambda_1^X)^k}{\Delta\xi}(1 + \operatorname{sgn}\lambda_1^X)^k$$

$$B_n = \frac{1}{\Delta t} + \frac{(\lambda_1^X)^k}{\Delta\xi}\operatorname{sgn}(\lambda_1^X)^k$$

$$C_n = \frac{1(\lambda_1^X)^k}{2\,\Delta\xi}(1 - \operatorname{sgn}\lambda_1^X)^k$$

$$D_n = (f_1^X + f_{31}^Y + f_1^L + f_1^P - D^* + aS_t)^k \quad (65)$$

Similar expressions are obtained for the rest of the equations to be integrated. At this stage, we observe that, in transonic flow about an airfoil, $\lambda_1^X$ is always positive above the airfoil (that is, for $\xi > 0$), whereas $\lambda_2^X$ is always negative below the airfoil (that is, for $\xi < 0$). Similarly, $\lambda_1^Y$ is positive and $\lambda_2^Y$ is negative everywhere. Finally, $\lambda_3^X$ in its regions of interest (that is, downstream of the shocks, where $S$ is different from zero) is positive for $\xi > 0$ and negative for $\xi < 0$. Consequently, the integration of $S$, $R'^X_1$, and $R'^X_2$, can be split into successive sweeps along $\eta = \text{const}$ lines, using the following coefficients:

For $S$,

| | $A_n$ | $B_n - 1\Delta t$ | $C_n$ | $D_n$ |
|---|---|---|---|---|
| $\xi < 0$ | 0 | $-\nu_3$ | $\nu_3$ | $f_4^X + f_4^Y$ |
| $\xi > 0$ | $-\nu_3$ | $\nu_3$ | 0 | $f_4^X + f_4^Y$ |

For $R'^X_1$,

| | | | | |
|---|---|---|---|---|
| $\xi < 0$ | $-\nu_1(1 + \operatorname{sgn}\nu_1)/2$ | $\nu_1 \operatorname{sgn}\nu_1$ | $\nu_1(1 - \operatorname{sgn}\nu_1)/2$ | $D_1^*$ |
| $\xi > 0$ | $-\nu_1$ | $\nu_1$ | 0 | $D_1^*$ |

For $R'^X_2$,

| | | | | |
|---|---|---|---|---|
| $\xi < 0$ | 0 | $-\nu_2$ | $\nu_2$ | $D_2^*$ |
| $\xi > 0$ | $-\nu_2(1 + \operatorname{sgn}\nu_2)/2$ | $\nu_2 \operatorname{sgn}\nu_2$ | $\nu_2(1 - \operatorname{sgn}\nu_2)/2$ | $D_2^*$ |

where, for simplicity, the superscript $k$ has been dropped, $\nu_i = \lambda_i^X/\Delta\xi$, and

$$D_1^* = f_1^X + f_{31}^Y + f_1^L + f_1^P - D^* + aS_t$$

$$D_2^* = f_2^X + f_{32}^Y + f_2^L + f_2^P - D^* + aS_t$$

Similarly, the integration of $R'^Y_1$ and $R'^Y_2$ is performed by sweeping along $\xi = \text{const}$ lines, using the following coefficients:

| | $A_n$ | $B_n - 1/\Delta t$ | $C_n$ | $D_n$ |
|---|---|---|---|---|
| For $R'^Y_1$ | $-\nu_1$ | $\nu_1$ | 0 | $f_1^Y + f_{31}^X + f_3^L + f_3^P - E^* + aS_t$ |
| For $R'^Y_2$ | 0 | $-\nu_2$ | $\nu_2$ | $f_2^Y + f_{32}^X + f_4^L + f_4^P - E^* + aS_t$ |

where now $\nu_i = \lambda_i^Y/\Delta\eta$.

By so doing, the integration procedure can be coded in a form that is perfectly symmetric with respect to the $\eta$ axis. It is also clear that, whenever either $A_n$ or $C_n$ vanishes, the integration reduces to the inversion of a two-diagonal matrix and inversions of three-diagonal matrices are needed only in two cases. No block inversion is needed either. Any sweeping in $\xi$ is vectorizable with respect to $\eta$, and vice versa. Finally, the integration of $S$ can be performed only where $S$ is different from zero, that is, downstream of the shocks. The number of operations per step is, thus, minimized.

Other speeding factors are the use of a local $\Delta t$ and of a Courant number larger than 1. If $D^*$ and $E^*$ [defined in Eq. (52)] are underrelaxed, that is, multiplied by ⅔ and added to ⅓ of their values at the previous step, the Courant number can be raised to values between 2.4 and 3.1 for the standard $(128 \times 32)$ mesh and higher values for coarser meshes.

## VIII. Boundary Conditions

In Fig. 1, a typical configuration of boundaries in both the physical plane and the mapped $\zeta$ plane is shown. *ABC* is an entry boundary. *AD* and *CE* are exit boundaries. *DFGHE* is a single boundary with different physical connotations: Along *DF* and *EH* continuity of the flow must be provided, whereas *FGH* is a rigid boundary, along which $v$ vanishes.

As we formerly did in all our λ-codes, we prescribe a fixed value of $\sigma = u/v$ and enforce constancy of total temperature and entropy at all points on the entry boundary.[10,11] In the present calculations, $\sigma$ is assumed equal to its value in the incompressible solution. Certain corrections to $\sigma$, proposed in Ref. 12 and used in Ref. 7, to make $\sigma$ more consistent with the conditions at infinity for a lifting airfoil, were found to produce no sizable changes in the computed values and were not introduced in the present code. This condition is not exact, but minor inaccuracies in $\sigma$ do not affect the flowfield on

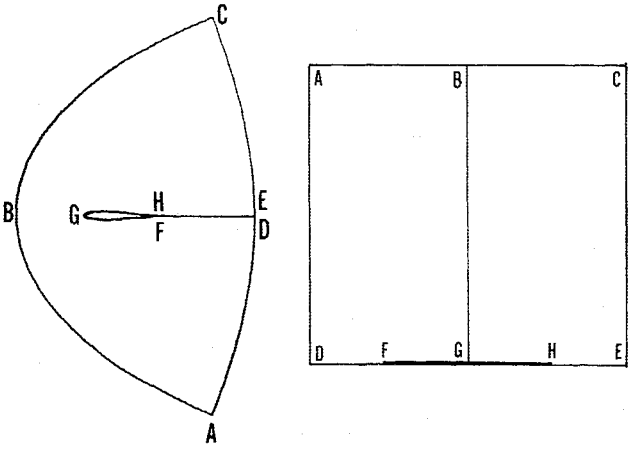


**Fig. 1 Boundaries of the computational and physical domains.**

the airfoil surface. The second condition expressed by the equation

$$a_\sigma^2 = a^2 + \delta(1+\sigma^2)v^2$$

or, after splitting $a$ and $v$ as shown in Sec. V,

$$0 = a'^2 + 2a^0 a' + \delta(1+\sigma^2)v'^2 + 2\delta v^0(1+\sigma^2)v' \tag{66}$$

is combined with the definition of $R_1'^Y$, which is correctly determined by the integration procedure (because it uses only information from inside)

$$R_1'^Y = a'/\delta + v' \tag{67}$$

From Eqs. (66) and (67),

$$v' = \{b^0 + \delta R_1'^Y - [(b^0 + \delta R_1'^Y)^2 - \epsilon(\delta R_1'^Y + 2a^0)R_1'^Y]^{1/2}\}/\epsilon \tag{68}$$

with

$$b^0 = a^0 - v^0(1+\sigma^2), \qquad \epsilon = 1 + \delta + \sigma^2$$

and $a'$ follows from Eq. (67). Finally, $R_2'^Y$ is computed as

$$R_2'^Y = R_1'^Y - 2v' \tag{69}$$

At the exit boundary, we assume that the pressure remains the same as initially prescribed. Since $p_t = 0$,

$$a(\ln p)_t/\gamma = a_t/\delta - aS_t = 0 \tag{70}$$

Therefore,

$$\Delta R_1'^X + \Delta R_2'^X = 2aS_t\Delta t \tag{71}$$

This condition provides $\Delta R_1'^X$ along $AD$ and $\Delta R_2'^X$ along $CE$. We must also provide correct values for $f_1^X$ along $AD$ and $f_2^X$ along $CE$, respectively. The domains of dependence of these quantities lie outside the computational domain; therefore, they cannot be approximated correctly by one-sided differences. On the other hand, they are used in $E^*$, as shown by Eq. (52); $E^*$, in turn, is used in the last two parts of Eq. (51). If we write Eq. (70) once more in the form

$$R_{1t}'^X + R_{2t}'^X + R_{1t}'^Y + R_{2t}'^Y - 4aS_t = 0$$

and use Eqs. (51) and (52), the equation

$$2(f_1^X + f_2^X + f_1^Y + f_2^Y) + f_1^L + f_2^L + f_3^L + f_4^L + f_1^P + f_2^P + f_3^P + f_4^P = 0 \tag{72}$$

is obtained; from it, either $f_1^X$ on $AD$ or $f_2^X$ on $CE$ can be determined.

On the airfoil surface ($FGH$), $v' = 0$; therefore, $R_1'^Y = R_2'^Y$ and

$$\Delta R_1'^Y = \Delta R_2'^Y \tag{73}$$

which yields $\Delta R_1'^Y$ since $\Delta R_2'^Y$ is properly determined by the integration procedure. On the airfoil surface, we must also determine $f_1^Y$, which is needed for $D^*$, as shown by the first part of Eq. (52); $D^*$, in turn, is used in the first two parts of Eq. (51). The domain of dependence of $f_1^Y$ lies inside the airfoil; therefore, this quantity cannot be approximated by one-sided differences. If we write the condition $v' = 0$ in the form

$$R_{1t}'^Y - R_{2t}'^Y = 0$$

and use the last two parts of Eq. (51), we obtain the following expression for $f_1^Y$:

$$f_1^Y = f_2^Y + f_4^L - f_3^L + f_4^P - f_3^P \tag{74}$$

having noted that

$$f_{32}^X - f_{31}^X = 2\lambda_3^X v_\xi' = 0$$

Along $DF$ and $EH$, $R_1'^Y(DF) = R_2'^X(EH)$ and $R_1'^Y(EH) = R_2'^X(DF)$. Therefore,

$$\Delta R_1'^Y(DF) = \Delta R_2'^Y(EH), \qquad \Delta R_1'^Y(EH) = \Delta R_2'^Y(DF) \tag{75}$$

At points $A$ and $C$, which are both entry and exit points, the initial conditions cannot be changed; consequently, $\Delta R_i'^X$ and $\Delta R_i'^Y$ ($i = 1, 2$) are forced to be equal to zero.

## IX. Trailing Edge Region in a $C$ Grid

A disadvantage of $C$ grids, as opposed to $O$ grids, is the loss of resolution in the region surrounding the trailing edge, where (if the airfoil ends in a wedge) there is a stagnation point and all variables undergo rapid changes, which cannot be properly described even by our finest mesh. As a consequence, there is a local loss of total energy, which is then propagated in the wake of the airfoil and shows up as an indentation in the isomach plots. Nevertheless, the local error in Mach number in the wake is only of the order of 0.001, and other values on the airfoil are not affected; therefore, all results obtained using a $C$ grid can be accepted.

For plotting and, more important, for computing $C_L$, $C_D$, and $C_M$, a further step is necessary. Without it, the diagrams of $M$ and $C_p$ on the airfoil show an abrupt, linear drop to stagnation values at the trailing edge. In computing the aerodynamic coefficients, $C_p$ is integrated around the airfoil. If a trapezoidal rule is used, the contribution of the trailing-edge region to the integrals is grossly miscalculated. Indeed, an incompressible flow analysis shows that near the trailing-edge stagnation point the velocity $u$ depends on the distance from the trailing edge $r$ through a fractional power law, $u = r^\alpha$, with $\alpha$ decreasing with the inner angle of the airfoil. Most of the change in $u$ may occur in a minimal fraction of the mesh interval; the same may be said of $M$ and $C_p$. To get a better approximation for such quantities and the aerodynamic coefficients, we divide each partial interval between the last mesh point on the airfoil and the trailing edge into 10 equal parts, and we compute the incompressible values of $q$, using the results as form factors to interpolate the primed values as well. The resulting values of $q$ are then used to obtain a detailed description of $C_p$, and the local contributions to $C_L$, $C_D$, and $C_M$ are computed accordingly. On the rest of the airfoil, the trapezoidal rule for integration can be used. If the shock falls in the last grid interval before the trailing edge, the procedure is confined to the partial aforementioned interval between the shock and the trailing edge.

## X. Computational Code for Subsonic Flows

In the absence of shocks, $S$ is constant throughout and need not be computed. We begin an integration step evaluating $\lambda$, according to Eq. (22) and $f$ according to Eq. (46) (without the $S$ terms), Eq. (47), and Eq. (48), at every point. In Eq. (46), the rule to approximate derivatives, mentioned at the beginning of Sec. VII, is applied. At boundary points on the airfoil surface and along $AD$, $CE$, the ill-defined $f$ is corrected according to Sec. VIII. Then, $R$ is integrated by sweeping along $\eta$ and $\xi = \text{const}$ lines. In this case, only bidiagonal matrices are to be inverted, and each sweep proceeds in the direction of increasing $\xi$ (or $\eta$) if $\lambda > 0$, in the opposite direction if $\lambda < 0$. In any case, the value of $\Delta R'$ at the first point of all integration sweeps is set equal to zero.

First, we integrate $R_1'^X$ for $\xi>0$ (above the airfoil), starting from the $BG$ line and sweeping in the direction of increasing $\xi$ along each $\eta=$ const line. Once the $CE$ line is reached, the boundary condition (71) is applied to get $\Delta R_2'^X$. Then $R_2'^X$ is integrated for $\xi<0$ (below the airfoil), starting from the $BG$ line and sweeping in the direction of decreasing $\xi$, and the boundary condition (71) is applied to get $\Delta R_1'^X$. The direction of sweeping is now reversed to complete the integration of $R_1'^X$ for $\xi<0$ and of $R_2'^X$ for $\xi>0$. The boundary line $ABC$ is not computed.

Similarly, a sweep in the direction of decreasing $\eta$ along each $\xi=$ const line is used to compute $\Delta R_2'^Y$. On reaching the airfoil surface or the common boundary $DF$ or $EH$, the boundary conditions (73) or (75), respectively, are applied to determine $\Delta R_1'^Y$, and the sweep is resumed in the opposite direction to determine $R_1'^Y$. When the outer boundary is reached, Eqs. (68) and (69) are used to get $R_2'^Y$ and $u$ is evaluated using $v$ and the prescribed value of $\sigma$.

## XI. Shock Calculation

For transonic calculations, where one or two shocks may appear, a shock-fitting procedure is added. The analysis outlined in the preceding sections remains unaltered and the procedure described in Ref. 2 is used, with minor changes, to fit the shocks. Briefly, we consider the following.

1) Cells having $\xi<0$ and containing a transition of $\lambda_1^X$ from positive to negative in the direction of increasing $\xi$, and cells having $\xi>0$ and containing a similar transition of $\lambda_2^X$ are marked as supports of a shock point. Unnecessary calculations are avoided: No search for shock points is made along $\eta=$ const lines that already contain two shock points or that lie above a line on which no shock point was found.

2) The tangent of the "shock angle" between the normal to the shock and the $\eta=$ const line at a shock point is defined by $-\Delta\xi/\Delta\eta$ using centered differences along the shock, except at the body, where it is forced equal to zero, and at the outermost point on a shock, where it is not computed at all. In what follows, $N_1$ denotes the $\xi$ component of the unit vector normal to the shock.

3) The shock Mach number $M$ is defined as

$$M=(\tilde{u}-W)/a \tag{76}$$

where $\tilde{u}$ is the normal velocity component and $W$ the shock velocity; both $\tilde{u}$ and $a$ are computed upstream of the shock. At a steady state, $W$ is obviously equal to zero.

4) The outermost point on a shock, where $M\cong 1$, is located by interpolating $M$ between the two adjacent grid nodes.[13]

5) The shock parameter

$$\Sigma=[a_B\pm\delta(u_A-u_B)]/a_A \tag{77}$$

(with the upper sign for the upper shock, and vice versa) can be defined using for $A$ and $B$ the grid nodes bracketing the shock on an $\eta=$ const line ($A$ always being on the low-pressure side and $B$ always on the high-pressure side). For all practical purposes, such an approximation is sufficient. Minor jumps in $\Sigma$ at a given shock point may occur, however, when the point moves from one grid interval to the next and, if the correct location of the point is very close to a node, the inaccuracy in $\Sigma$ may trigger a minute, but never damped, oscillation of the computed shock point about its correct value. A smooth transition of $\Sigma$ when the shock point passes from one cell to an adjacent one is obtained by assuming that $A$ and $B$ lie on the shock itself, and by extrapolating any function $w(w=S, a, u, v)$ as in the following example, written for $\xi>0$ and $A$.

Let $\xi_s$ be the value of $\xi$ at the shock point (which lies between the points $\xi_n$ and $\xi_{n+1}$) and

$$\epsilon=(\xi_s-\xi_n)/(\xi_{n+1}-\xi_n),\qquad \epsilon_1=(\xi_s-\xi_n)/(\xi_n-\xi_{n-1})$$

$$\epsilon_2=(\xi_s-\xi_{n-1})/(\xi_{n-1}-\xi_{n-2}) \tag{78}$$

$$w_1=w_n+\epsilon_1(w_n-w_{n-1}),\qquad w_2=w_{n-1}+\epsilon_2(w_{n-1}-w_{n-2}) \tag{79}$$

$$w_A=\epsilon w_1+(1-\epsilon)w_2 \tag{80}$$

If, for the sake of simplicity, we assume that the nodes are equally spaced, it is easy to verify that, for $\epsilon$ approaching 0 or 1, not only $w$ but $dw/d\xi$ as well are continuous.[14]

6) Since the Rankine-Hugoniot conditions relate $\Sigma$ and the shock Mach number $M$ in the following form:

$$\Sigma=\{[(\gamma M^2-\delta)(1+\delta M^2)]^{1/2}+\delta(M^2-1)N_1\}/(1+\delta)M \tag{81}$$

$M$ can be obtained by inverting Eq. (81), and $W$ is computed from Eq. (76). Finally, the shock abscissa $\xi_s$ is incremented by $W/N_1\cdot\Delta t$, where $\Delta t$ is evaluated locally.

7) The Rankine-Hugoniot conditions are then applied to revaluate $S$, $a$, $u$, and $v$ at point $B$. Consistently with the extrapolations just described, the values at the node immediately downstream of the shock are interpolated using the values at $B$ and the values at the next subsonic node.

8) The entire shock calculation is made using the physical values of $S$, $a$, $u$, and $v$. Primed values are then obtained by using Eq. (33).

9) Minor wiggles in the shock geometry may appear as a consequence of minor inconsistencies among the locations of shock points at the instant of creation. Since the direction of the normal to the shock is obtained using centered differences, such wiggles cannot be reabsorbed. In Ref. 13, when we started from the analysis of a normal shock in a channel, it was concluded that two-dimensional oblique shocks should tend to remain smooth; wrinkles should tend to disappear if they ever formed by accident. The numerical interpretation of this physical fact cannot be applied in the present code as it was. The same physical argument, however, can be used to conclude that the smoothing "channel effect" is the stronger, the higher the curvature of the computed shock geometry. Consequently, a simple, physically consistent smoothing device is obtained by correcting $\Sigma$ by a minimal fraction (of the order of 0.001) of the curvature of the shock in the computational plane. The initial wiggles are thus reabsorbed, without affecting the steady-state geometry of the shock.

## XII. Computational Code for Transonic Flows

The code outlined in Sec. X is modified for transonic flows with shocks, as follows. The entropy is still considered constant at all nodes, except those lying on $\eta=$ const lines issuing from shock points downstream of the shocks. As in the subsonic case, the integration step begins by evaluating $\lambda$ according to Eq. (22) and $f$ according to Eqs. (46–48), at every point. The same rule to approximate derivatives and the same corrections at boundaries as in Sec. X apply. Bidiagonal matrices are used to update $R_1'^X$ above the airfoil and $R_2'^X$ below it; bidiagonal matrices are also used to update $R_1'^Y$ and $R_2'^Y$. Tridiagonal matrices are used to update $R_1'^X$ below the airfoil and $R_2'^X$ above it. The entropy, in the regions where it is different from zero, is updated inverting bidiagonal matrices.

To avoid transmitting spurious information across a shock, we set $A_n=0$ for $R_1'^X$ and $\xi>0$ and $C_n=0$ for $R_2'^X$ and $\xi<0$ at the first two nodes downstream of the shock. Similar provisions should be taken for possible crossing of $\xi=$ const lines. Not to complicate the logic and increase the running time, we simply force $A_n=0$ for $R_1'^Y$ and $C_n=0$ for $R_2'^Y$ at two points on either side of the shock along its $\eta=$ const line.

## References

[1]Schmidt, W. and Jameson, A., "Eulers Solvers as an Analysis Tool for Aircraft Aerodynamics," *Advances in Computational Transonics*, Pineridge Publ., 1985, pp. 371–404.

[2]Moretti, G., "A Technique for Integrating Two-Dimensional Euler Equations," *Computers and Fluids*, Vol. 15, 1986, pp. 59–75.

[3]Moretti, G., "Fast Euler Solver for Steady One-Dimensional Flows," *Computers and Fluids,* Vol. 13, 1985, pp. 61–81.

[4]Dadone, A. and Napolitano, M., "Accurate and Efficient Solutions of Compressible Internal Flows," *Journal of Propulsion and Power,* Vol. 1, Nov.–Dec. 1985, pp. 456–463.

[5]Moretti, G., "A Fast Euler Solver for Steady Flows," *Proceedings of the AIAA 6th Computational Fluid Dynamics Conference,* AIAA, New York, MA, 1983, pp. 357–362.

[6]Dadone, A., "A Quasi-Conservative COIN Lambda Formulation," *Lecture Notes in Physics,* Vol. 264, pp. 200–204.

[7]Moretti, G. and Lippolis, A., "Transonic Airfoil and Intake Calculations," GAMM Workshop, Rocquencourt, France, June 1986 (to appear in *Notes on Num. Fl. Dyn.,* Vieweg Publ., 1987).

[8]Beam, R. M. and Warming, R. F., "An Implicit Factored Scheme for the Compressible Navier-Stokes Equations," *AIAA Journal,* Vol. 16, April 1978, pp. 393–402.

[9]Dadone, A. and Napolitano, M., "A Perturbative Lambda Formulation," *AIAA Journal,* Vol. 24, 1986, pp. 411–417.

[10]Pandolfi, M. and Zannetti, L., "Some Permeable Boundaries in Multidimensional Unsteady Flows," *Lecture Notes in Physics,* Vol. 90, 1978, pp. 439–446.

[11]Moretti, G., "A Physical Approach to the Numerical Treatment of Boundaries in Gas Dynamics," NASA CP 2201, 1981, pp. 73–95.

[12]Thomas, J.L. and Salas, M.D., "Far-Field Boundary Conditions for Transonic Lifting Solutions to the Euler Equations," *AIAA Journal,* Vol. 24, July 1986, pp. 1074–1080.

[13]Moretti, G., "Floating Shock Fitting Technique for Imbedded Shocks in Unsteady Multidimensional Flows," *Proceeding of the 1974 Heat Transfer and Fluid Mechanics Institute,* edited by L. R. Davis and R. E. Wilson, Stanford Univ. Press, CA, 1974, pp. 184–201.

[14]Moretti, G., "Thoughts and Afterthoughts About Shock Computations," Polytechnic Inst. of Brooklyn, New York, Rept. PIBAL 72-73, 1972.